Star-disk magnetospheric interaction with non-dipolar stellar field

Filip Cieciuch[1] and Miljenko Čemeljić[2,3]

1. Faculty of Physics, University of Warsaw, Pasteura 5, 02–093 Warsaw, Poland
2. Nicolaus Copernicus Astronomical Center of the Polish Academy of Sciences, Bartycka 18, 00–716 Warsaw, Poland
3. Institute of Astronomy and Astrophysics, Academia Sinica, P.O. Box 23–141, Taipei 106, Taiwan

In our study, we investigate non-dipolar geometries of stellar magnetic field. We perform resistive and viscous magneto-hydrodynamical simulations of a star-disk system and compare the results for the dipole, quadrupole, and octupole stellar magnetic fields. With the column positioned closer to the equatorial plane in the octupole case, runs tend to be more stable and reach the quasi-stationarity easier than in the cases with the stellar dipole field. In the quadrupole case, the matter flows directly onto the stellar equator, similar to the purely hydrodynamic case.

1 Introduction

Mass in the accretion disk around a star can behave in different ways: it can fall directly at the equator of a star or form an accretion column at a higher latitude, but it can also escape from the vicinity of a star in the form of stellar wind and a conical or axial outflow. Which scenario is realized in our simulations depends on free parameters such as resistivity, viscosity, and stellar rotation rate, but it also depends on the geometry and strength of the stellar magnetic field. In the simulations presented in Čemeljić (2019) the interaction between a thin accretion disk and a rotating stellar surface with the dipolar stellar magnetic field was investigated. Here we extend this research to the non-dipolar fields.

2 Numerical Setup – of Dipole, Octupole, and Quadrupole stellar field

We use the PLUTO v.4.1 code (Mignone et al., 2007) to perform 2D-axisymmetric star-disk simulations in a half of the latitudinal plane. The resolution is $R \times \theta = [217 \times 100]$ grid cells in spherical coordinates, with the physical domain extending to the maximal radius of 30 stellar radii in a logarithmically stretched radial grid, and from the pole to the equatorial plane in an uniform co-latitudinal grid. The initial disk is set following Kluzniak & Kita (2000) purely hydro-dynamical solution, onto which we add the stellar magnetic field:

$$\vec{B}_{\rm dip} = 2\mu\frac{\cos\theta}{R^3}\hat{R} + \mu\frac{\sin\theta}{R^3}\hat{\theta},\ \vec{B}_{\rm quad} = \frac{3}{2}\frac{\mu}{R^4}(3\cos^2\theta - 1)\hat{R} + 3\frac{\mu}{R^4}\sin\theta\cos\theta\hat{\theta},$$
$$\vec{B}_{\rm oct} = 2\mu\frac{\cos\theta}{R^5}(5\cos^2\theta - 3)\hat{R} + \frac{3}{2}\mu\frac{\sin\theta}{R^5}(5\cos^2\theta - 1)\hat{\theta},$$

where $\mu = 0.7$ is a free parameter in our simulations, determining the field strength. So defined initial fields are of the same strength in the equatorial plane just in front of the star, at about $1.5R_\star$, inside the initial disk gap. We set the slowly rotating star,

with $\Omega_\star/\Omega_{\rm br} = 0.1$. The viscosity and resistivity in the disk are parameterized by the Shakura-Sunyaev alpha-viscosity prescription as $\alpha c^2/\Omega$, where c is the isothermal sound speed $c = \sqrt{P/\rho}$, defined by the ratio of pressure and density, and Ω is the disk angular speed at some distance from the star. We set both coefficients $\alpha_{\rm v} = \alpha_{\rm m} = 1$. Our setup is detailed in Čemeljić (2019), where is also given a table with the scaling for different objects like white dwarfs and neutron stars. We compare the resulting geometry of the flow, mass accretion rates and angular momentum fluxes.

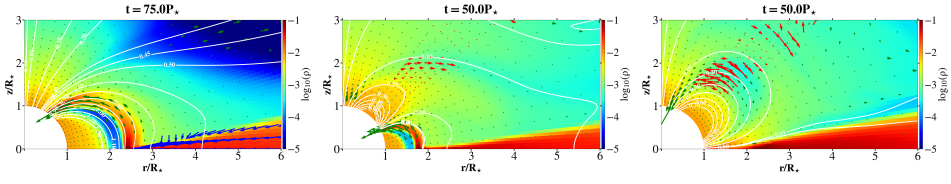

Fig. 1: Zoom into the vicinity of the star in quasi-stationary results in our simulations in the dipole, octupole, and quadrupole field cases, left to right, respectively, with time measured in stellar rotation periods. The density is shown in the logarithmic color grading, poloidal magnetic field lines are shown with white solid lines, and vectors of poloidal velocity (normalized to the Keplerian velocity at the stellar equatorial surface) are multiplied with the factors 15 (in the disk) and 3 (in the corona).

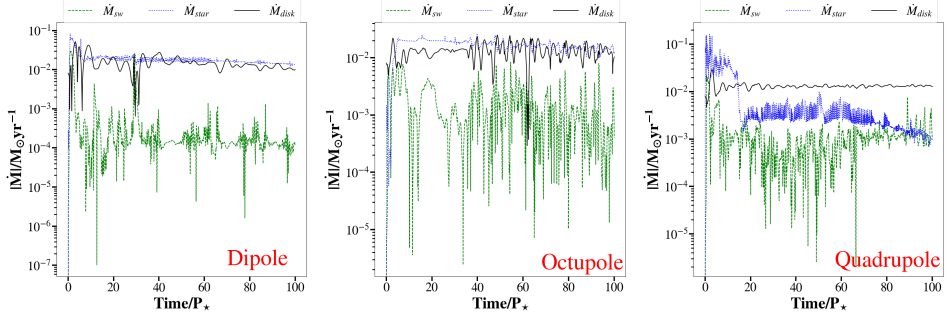

Fig. 2: Mass flux $\dot{M} = \rho v_{\rm p}$ in units of $\dot{M}_0 = \rho_0 R_\star^2 v_0$ (defined at stellar equator): across the disk at $R = 15R_\star$ ($\dot{M}_{\rm disk}$), at $R_\star$ onto the star ($\dot{M}_{\rm star}$) and into the stellar wind at $R = 15R_\star$ ($\dot{M}_{\rm SW}$) for the dipole, octupole, and quadrupole geometry of the initial magnetic field. In the quadrupole field case, the fraction of the disk mass accreted onto the star is smaller than in the dipole and octupole cases.

3 Results and Conclusions

In the cases of dipole and octupole magnetic field an accretion column is formed, with the mass accreting onto the star along the magnetic field lines – see Fig. 1. In the octupole case the footpoint of the magnetic field lines is closer to the stellar equator than in the dipole case, and in the quadrupole case, the matter flows directly onto the stellar equator, similar to the purely hydrodynamic case. The octupole runs tend to be more stable and reach the quasi-stationarity easier than the dipole.

The quasi-stationary state in our simulations is reached few stellar rotations after

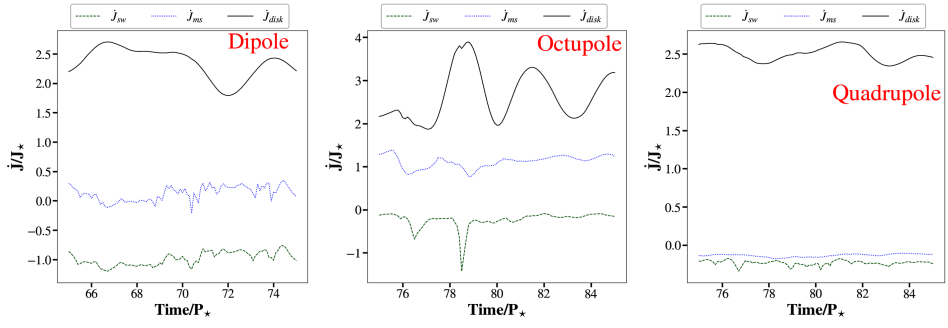

Fig. 3: Angular momentum flux in units of $\dot{J}_\star = 0.2 M_\star R_\star^2 \Omega_\star$, during the quasi-stationary interval in our simulations computed in the "stellar wind" above the disk, $\dot{J}_{\rm sw}$ (dashed green line) and across the disk $\dot{J}_{\rm disk}$ (solid black line) are computed at the half of the computational box $R = 15 R_\star$. The "magnetospheric" angular momentum flux $\dot{J}_{\rm ms}$ (dotted blue line) we compute above the disk, at the distance $R = 1.5 R_\star$, at which the initial magnetic field strength is the same in all the three geometries.

the relaxation from the initial and boundary conditions – see Fig. 2. In the dipole and octupole cases a similar fraction of the mass from the disk is accreted onto the star, and in the quadrupole case, less of the mass from the disk accretes onto the star. In Fig. 3 we show the angular momentum flux, computed accross the three surfaces. The first two are computed at the half of the computational box $R = 15 R_\star$: in the "stellar wind" above the disk $\dot{J}_{\rm sw}$ and accross the disk $\dot{J}_{\rm disk}$. The third, "magnetospheric" angular momentum flux $\dot{J}_{\rm ms}$ is computed at $R = 1.5 R_\star$, where the initial magnetic field strength is the same in all the three geometries. Our preliminary results show that $\dot{J}_{\rm sw}$ in all the geometries is of the same order, with the largest amount in the dipolar case. Of the three investigated cases, the octupole contains the largest amount of $\dot{J}_{\rm ms}$. The amount of angular momentum flux in the disk is of the same order in all the cases, as expected for the same initial and boundary condition used in the simulations. In the future work we will investigate the trends in the results with other parameters, like it was done in Čemeljić (2019) for the dipole field case.

Acknowledgements. This work is funded by the Polish NCN grant 2019/33/B/ST9/01564. We thank ASIAA (XL cluster) in Taipei, Taiwan and NCAC (CHUCK cluster) in Warsaw, Poland, for access to Linux computer clusters used for high-performance computations. We thank the PLUTO team for the possibility to use the code.

References

Kluzniak, W., Kita, D., *arXiv e-prints* astro-ph/0006266 (2000)

Mignone, A., et al., *ApJS* **170**, 1, 228 (2007)

Čemeljić, M., *A&A* **624**, A31 (2019)